Title
Determining Atomic-Scale Structure and Composition of Organo-Lead Halide Perovskites by Combining High-Resolution X-ray Absorption Spectroscopy and First-Principles Calculations

Journal
ACS Energy Letters, 2(5)

ISSN
2380-8195

Authors
Drisdell, Walter S
Leppert, Linn
Sutter-Fella, Carolin M
et al.

Publication Date
2017-05-12

DOI
10.1021/acsenergylett.7b00182

Peer reviewed

Title: Determining atomic-scale structure and composition of organo-lead halide perovskites by combining high-resolution X-ray absorption spectroscopy and first-principles calculations

Author List: Walter S. Drisdell[1]*, Linn Leppert[2,3], Carolin M. Sutter-Fella[1], Yufeng Liang[2], Yanbo Li[1], Quynh P. Ngo[4,5], Sheraz Gul[6], Thomas Kroll[7], Dimosthenis Sokaras[7], Ali Javey[4], Junko Yano[6], Jeffrey B. Neaton[2,3,8], Francesca M. Toma[1]*, David Prendergast[2]*, Ian D. Sharp[1]*

[1]Chemical Sciences Division, Lawrence Berkeley National Laboratory, Berkeley, CA 94720, USA.

[2]Molecular Foundry, Lawrence Berkeley National Laboratory, Berkeley, CA 94720, USA.

[3]Department of Physics, University of California, Berkeley, CA 94720, USA.

[4]Department of Electrical Engineering and Computer Sciences, University of California, Berkeley, CA 94720, USA.

[5]Materials Sciences Division, Lawrence Berkeley National Laboratory, Berkeley, CA 94720, USA.

[6]Molecular Biophysics and Integrated Bioimaging Division, Lawrence Berkeley National Laboratory, Berkeley, CA 94720, USA.

[7]Stanford Synchrotron Radiation Lightsource (SSRL), SLAC National Accelerator Laboratory, Menlo Park, CA 94025, USA.

[8]Kavli Energy NanoScience Institute at Berkeley, Berkeley, CA 94720, USA.

* = corresponding author

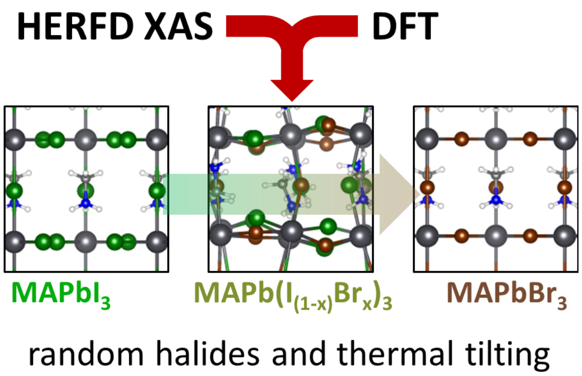

Abstract:

We combine high energy resolution fluorescence detection (HERFD) X-ray absorption spectroscopy (XAS) measurements with first-principles density functional theory (DFT) calculations to provide a molecular scale understanding of local structure, and its role in defining optoelectronic properties, in $CH_3NH_3Pb(I_{1-x}Br_x)_3$ perovskites. The spectra probe a ligand field splitting in the unoccupied *d* states of the material, which lie well above the conduction band minimum and display high sensitivity to halide identity, Pb-halide bond length, Pb-halide octahedral tilting, as well as the organic cation. We find that the halides in these mixed compositions are randomly distributed, rather than having preferred octahedral sites, and that thermal tilting motions dominate over any preferred structural distortions as a function of halide composition. These findings demonstrate the utility of the combined HERFD XAS and DFT approach for determining structural details in these materials and connecting them to optoelectronic properties observed by other characterization methods.

Hybrid organic-inorganic halide perovskites have attracted intense interest as advanced semiconductors for a range of optoelectronic applications, including in photovoltaics, where perovskite solar cell power conversion efficiencies now exceed 22%.[1] Despite swift progress in the field, there is a pressing need to connect device-relevant optoelectronic properties to atomic-scale structure, particularly in compositionally complex compounds. . For example, while methylammonium lead halide perovskites, $CH_3NH_3Pb(I_{1-x}Br_x)_3$ ($MAPb(I_{1-x}Br_x)_3$), have been intensively investigated, precise crystal structures – derived from volume- and time-averaged diffraction measurements – are only available for the pure halide compounds ($MAPbI_3$ and $MAPbBr_3$).[2-3] Existing diffraction studies of the mixed halide compositions do not show evidence for phase separation, but these measurements provide macroscopically averaged lattice parameters[4] and it is unclear whether halide atoms are randomly distributed or preferentially ordered in any given PbX_6 (X=I, Br) octahedron. Furthermore, while density functional theory (DFT) studies can determine energetically favorable local structures of mixed halide perovskites,[5] the rotational dynamics of the methylammonium (MA) molecule are generally not taken into account in static DFT calculations. Indeed, structural relaxations for fixed MA orientations can result in spurious and unphysical distortions of the PbX_6 octahedra that are largely averaged out at finite temperature.[6] Such distortions, as well as molecular-scale distributions of halides and cations, could have a large impact on material properties including band gaps, carrier lifetimes, and device stability.[6-9] An accurate, self-consistent determination of the molecular-scale structure in these systems, to connect with observed optoeletronic properties, is needed to enable directed design of compositionally complex, bandgap engineered perovskite semiconductors capable of the high efficiency energy conversion necessary for tandem photovoltaic applications.

To this end, we present an X-ray absorption spectroscopy (XAS) and first principles DFT study of $MAPb(I_{1-x}Br_x)_3$ perovskites as a function of composition. XAS probes electronic excitations from core orbitals into the unoccupied band structure of the excited material, providing both elemental and electronic selectivity due to the associated dipole selection rule, which dictates the angular momentum of the final state orbital. Given the small spatial extent (~0.1 Å) of the resonantly excited electronic core orbitals, XAS provides highly local information about the electronic structure near the excited atom, which is often strongly coupled to the atomic structure via coordination and associated hybridization with orbitals on neighboring atoms. To interpret the spectral signatures of these effects, we employ first-principles DFT calculations of the XAS. Beginning with the experimentally derived $MAPbI_3$ and $MAPbBr_3$ structures, these calculations assess the specific spectral sensitivity to halide identity, bond lengths, and octahedral tilts. These tests then inform the interpretation of calculated XAS for several candidate structural models for mixed halide compositions derived from ground-state DFT calculations. These spectral simulations reveal individual electronic transitions responsible for particular spectral features, and can isolate contributions from specific atoms in the material, elucidating structural details that are probed by the XAS experiment. By combining experiment and computation in this way, we demonstrate sensitivity to structural information on the molecular scale, including halide identity, Pb-halide bond lengths, and octahedral tilting. Thus, pairing XAS and DFT can connect local atomic structure to optoelectronic properties determined by other characterization methods, informing design rules for efficient and stable perovskite devices.

XAS was collected at the Pb L_{III}-edge (see SI for details) for $MAPb(I_{1-x}Br_x)_3$ perovskites across the complete halide composition space ($0 \leq x \leq 1$). Fluorescence yield XAS, as is typically employed, is dominated by lifetime broadening effects, as shown in Figure 1a, making it difficult to discern the nature of the spectral differences with respect to composition and precluding comparison to computed XAS, which can neglect lifetime broadening. To circumvent this, we employed high energy resolution fluorescence detection (HERFD) XAS, using an emission spectrometer tuned to the Pb Lβ-5 emission line. By isolating the peak of a single emission line, the HERFD XAS technique eliminates much of the intrinsic lifetime broadening, resulting in sharper, more well-defined spectral features.[10]

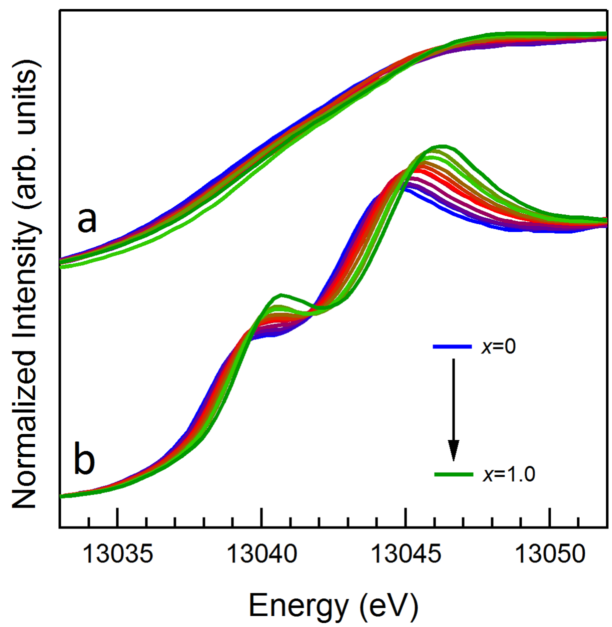

Figure 1: (a) Standard and (b) HERFD XAS spectra for $CH_3NH_3Pb(I_{1-x}Br_x)_3$ as a function of x, in increments of ~0.1 (see SI for details).

As shown in Figure 1b, HERFD XAS reveals a spectral feature in the middle of the rising absorption edge, as well as a distinct feature at the top of the main edge, for the $MAPb(I_{1-x}Br_x)_3$ composition series. Both spectral features blueshift with increasing Br content (indicated by x); the rising edge feature shifts from 13039.9 eV to 13040.8 eV (+0.9 eV), and the main edge feature shifts from 13044.7 eV to 13046.2 eV (+1.5 eV) for $MAPbI_3$ and $MAPbBr_3$, respectively. For intermediate compositions, both features are positioned between their corresponding extrema. Spectra for the mixed halide materials, however, cannot be accurately described by a linear combination of the spectra of $MAPbI_3$ and $MAPbBr_3$ (Figure S3). This finding implies that the intermediate compositions form well-mixed single phases, rather than segregated pure halide phases, as supported by prior diffraction studies.[4]

To determine the origin of the spectral shifts with halide composition, we employed first-principles DFT calculations, using the PBE functional, within the excited electron and core hole (XCH) approach[11] (details in SI). A comparison between experimental and computed spectra for $MAPbI_3$ and $MAPbBr_3$ is shown in Figure 2. The computed spectra for these pure halide compounds are based on averaged structures deduced from diffraction studies.[3, 12-13] Despite employing HERFD XAS, the experimental spectra display larger broadening than the first-principles computed spectra. This effect is expected, given that these specific calculations are for static structural models and neglect nuclear motion and associated vibronic coupling; the effect of thermal motion on the spectra is discussed in additional detail below. Aside from the degree of broadening, the agreement between computed and experimental spectra is excellent. Using a single reference spectrum for energy calibration[14] (in this case, the spectrum of $MAPbI_3$), the computations reproduce experimental spectral positions and relative intensities for both perovskite compounds, including the sharpened rising edge feature at 13040.8 eV for $MAPbBr_3$ compared to that at 13039.9 eV for $MAPbI_3$. Again, under fluorescence yield detection, this spectral difference would be obscured by lifetime broadening effects.

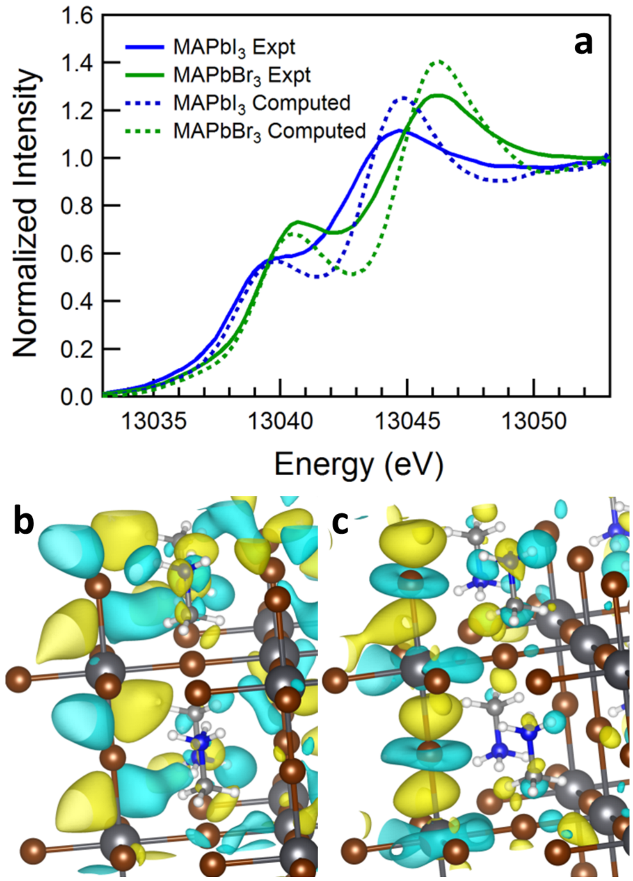

Figure 2: (a) Comparison of experimental (solid lines) HERFD XAS and computed (dotted lines) XAS for $MAPbI_3$ (blue) and $MAPbBr_3$ (green). Also shown are excited state electronic orbitals which dominate contributions to (b) the rising edge near 13041 eV and (c) the main edge near 13046 eV, in the computed XAS for $MAPbBr_3$. Pb are dark grey, Br are brown, N are blue, C are light grey, and H are white. The opposing phases of the orbitals are shown in yellow and cyan.

The XCH spectral calculations also provide final-state excited electron orbitals for each transition in the spectrum. Excited electron orbitals for the strongest excitations in the rising edge and main edge features for the case of $MAPbBr_3$ are shown in Figure 2b and 2c. Both orbitals show *d*-*d* hybridization between Pb and Br; the rising edge orbital (Fig. 3a) exhibits d_{xz} character, whereas the main edge orbital shows d_{z^2}character (Fig. 3b). The spectral features can therefore be understood in terms of ligand field theory. In octahedral coordination symmetry, the manifold of atomic *d*-orbital energies splits due to ligand repulsion, with $d_{z^2}$and $d_{x^2-y^2}$orbitals raised in energy since they are oriented along the octahedral bonds, and the d_{xy}, d_{xz} and d_{yz}

orbitals lowered in energy since they are non-bonding, i.e., oriented between the bonds. The energy splitting observed between the spectral features in the perovskite spectra is therefore a ligand field splitting. Interestingly, the electronic orbital components of the final states probed here (based on Pb 2p → 6d transitions) lie ~10 eV above the Fermi level (Figure S4) and, therefore, are not directly involved in the photovoltaic function of the perovskite materials. As demonstrated below, however, these orbitals are highly sensitive to bond lengths, halide electronegativity, and octahedral tilting, and can be used as a proxy to deduce subtle details of the local atomic structure. Therefore, combining HERFD XAS measurements with first-principles DFT simulations provides an important validation of the local structural and compositional models required for DFT-based predictions of optoelectronic properties. Comparisons to measurements of the optoelectronic properties of the same materials using other characterization methods (e.g., photoluminescence) will enable the connection of structural and compositional degrees of freedom with valence band structure, revealing effective design strategies to control optoelectronic properties in perovskites more generally.

There are several structural differences between $MAPbI_3$ and $MAPbBr_3$. At ambient temperature, the $MAPbI_3$ structure adopts a tetragonal phase with I4/mcm symmetry, in which the PbI_6 octahedra are rotated about the *c*-axis with respect to the cubic Pm-3m phase of $MAPbBr_3$.[2] In addition, the Pb-Br bonds (2.99 Å) are ~0.20 Å shorter than Pb-I bonds (3.17 Å apical, 3.19 Å equatorial), resulting in 5% smaller lattice parameters per formula unit (6.28 Å for $MAPbI_3$ versus 5.97 Å for $MAPbBr_3$). The Pb-I and Pb-Br bonds also show different degrees of ionic character due to the larger electronegativity of Br (2.96 Pauling units) versus I (2.66 Pauling units)[15], which affects the electronic structure around the Pb centers. To isolate the effect of each of these degrees of freedom on the XAS, we performed a systematic series of spectral computations, utilizing structures labelled P1 through P5, as shown in Figure 3. Starting with the tetragonal $MAPbI_3$ structure (P1), we aligned (i.e. un-rotated) the PbI_6 cages, converting it to the higher symmetry cubic Pm-3m phase (P2). This has a very small effect on the spectrum, introducing a blueshift of ~0.1-0.2 eV in the rising edge feature. Next, we replaced the I^- ions with Br^- ions, while keeping the rest of the structure fixed (P3). This drastically changes the spectrum, blueshifting the rising edge feature by 1.4 eV, which is larger than the experimentally observed blueshift of 0.9 eV. The main edge feature, on the other hand, is blueshifted by only 0.8 eV, compared to the 1.5 eV blueshift observed experimentally. Shortening the Pb-Br bonds to the experimental lengths for $MAPbBr_3$ (P4) shifts the spectral features to match experiment; the rising edge feature is redshifted by 0.5 eV and the main edge feature is further blueshifted by 0.7 eV. Finally, we tilted the $MAPbBr_3$ octahedra such that the resulting structure (P5) has Pnma symmetry but approximately retains the bond lengths of P4. This introduces significant broadening in the main edge feature and also redshifts and broadens the rising edge feature.

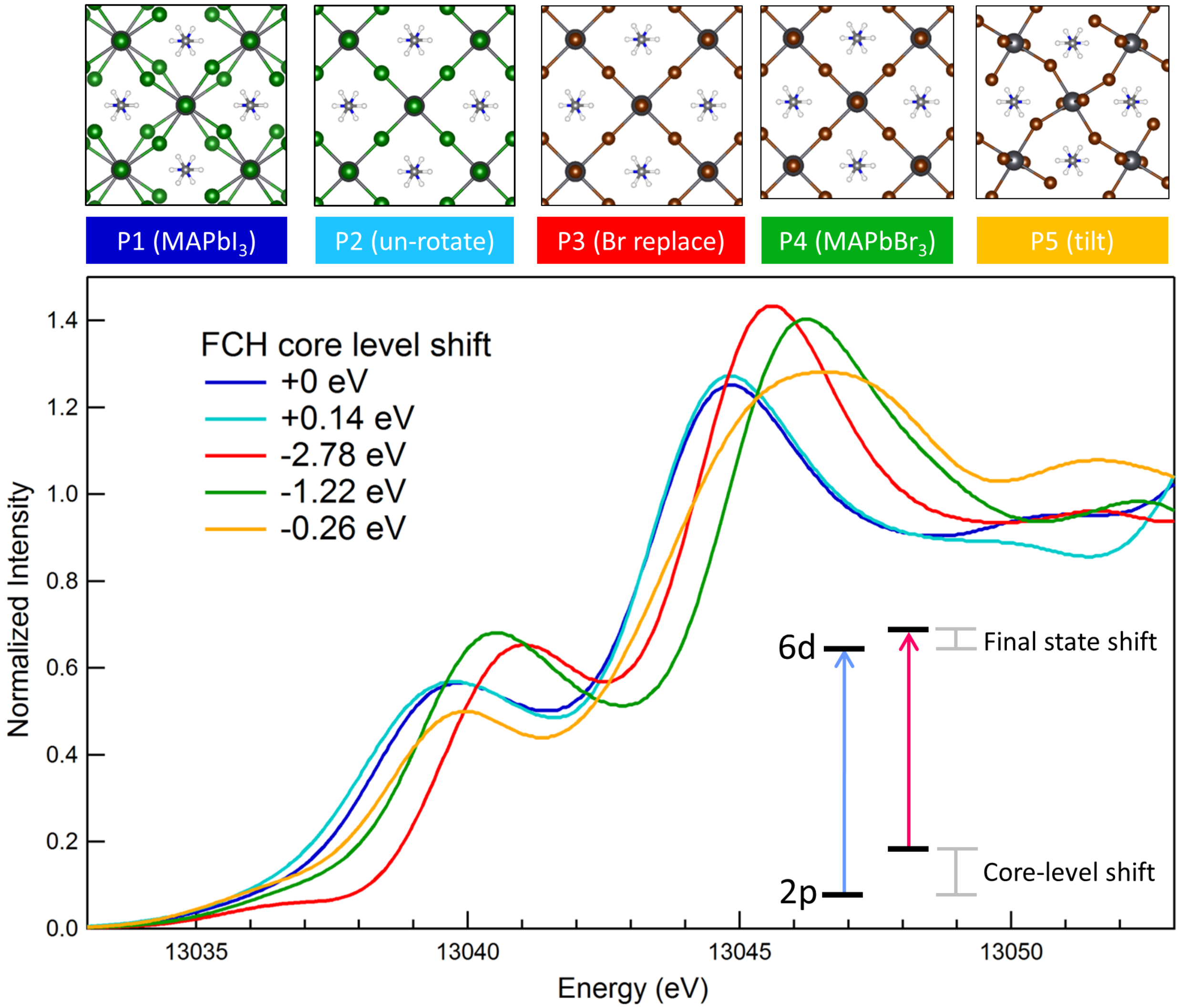

Figure 3: Comparison of computed XAS for $MAPbI_3$ (P1, blue), the same structure with un-rotated PbI_6 octahedra (P2, cyan), I replaced with Br without relaxation (P3, red), Pb-Br bond lengths reduced to the experimental values for $MAPbBr_3$ (P4, green), and $MAPbBr_3$ with tilted octahedra (P5, orange). Pb are dark grey, I are green, Br are brown, C are light grey, N are blue, and H are white. Computed FCH core level shifts for each structure are also listed, relative to P1. Inset: A schematic representation of the potentially competing effects of core-level and final-state shifts in defining the X-ray absorption energy.

This computational assessment demonstrates that HERFD XAS should be highly sensitive to halide identity, Pb-halide bond length, and octahedral tilting, but less sensitive to bond-length preserving rotations of the Pb-halide cage. Note that we assume that XAS sensitivity to the lattice parameters is implicit, given the strong connection between the volume of the crystal unit cell and the local degrees of freedom considered here. The actual spectral response to these factors arises from a combination of shifts in the energies of the d_{z^2} and d_{xz} final states (pictured in Figure 2) – due to varying ligand field effects about the Pb atom – and shifts in the Pb 2p core orbital energies due to varying degrees of oxidation by the halides. This is illustrated by the difference between the P3 and P4 spectra: when the Pb-halide bond length is shortened, the d_{z^2} states in the main edge – which are oriented along the bonds – are expected to undergo a significant shift to higher energy, while the d_{xz} states in the rising edge should experience a much more moderate shift to higher energies since they are oriented away from the bond axes. The computed spectra, however, show a redshift in the rising edge feature for P4 versus P3, implying that final state shifts are offset by shifts in the core 2p orbitals. We quantified these core level shifts using the full core hole (FCH) DFT method (details in SI), showing that P4 has a 2p core level 1.56 eV shallower (spectral redshift) than that of P3, likely due to the reduced ionicity (and hence Pb oxidation) of the shorter bond length in P4. The d_{z^2} states in the main edge are sensitive enough to bond length to dominate the spectral response in the main edge, but for the less sensitive d_{xz} states in the rising edge, the Pb core level shift dominates.

The sensitivity to octahedral tilts (P5) deserves special note as it is likely that similar tilting motions occur thermally under experimental conditions; indeed, DFT studies show that octahedral tilts should correlate with rotations of the MA molecule.[16-18] The tilts in the P5 structure disrupt the strong d_{z^2} and d_{xz} couplings, breaking degeneracy and broadening both the main edge and rising edge spectral features into shapes that more closely resemble experimental spectra. The rising edge feature is also redshifted by ~0.65 eV as compared to P4, resulting in a splitting larger than that observed in experiment and implying that the tilts in the P5 structure are more severe than the actual thermal motions under ambient conditions. The implications of thermal tilting motions are discussed further below.

Examining how the ligand field effects manifest in mixed-halide structures is more difficult, due to the lack of definitive structural models for mixed-halide compositions based on experimental measurements. We employed DFT within the Perdew-Burke-Ernzerhof (PBE) approximation as implemented in VASP[19] to determine possible structures to use for computing XAS. Static DFT calculations neglect the thermal motion of the MA molecule and therefore introduce spurious distortions of the PbX_6 octahedra that arise as a result of choosing fixed orientations of the MA molecule. The energetic barrier to rotation for the MA molecules is expected to be as small as 10 – 20 meV,[20] implying that they rotate freely at ambient temperature, leading to random, uncorrelated orientations.[21] To obtain reliable structures it is therefore appropriate to treat the cation site as isotropic. To this end, we use the virtual crystal approximation (VCA)[22] to replace MA by a spherical "pseudoatom" such that after full structural relaxation the volume of the unit cell matches the experimental volume. This approach accurately reproduces lattice parameters derived from X-ray diffraction studies of mixed-halide compositions, as well as lead-halide bond lengths for the pure compositions (see SI for details).

After the DFT structural relaxation, we replaced the pseudoatoms with MA cations to properly capture interactions between the MA and the electronic final states for the XAS transitions (see SI for details). Three compositions were examined: $x = 0.4$, $x = 0.6$, and $x = 0.8$, with randomized halide distributions for each. For the $x = 0.6$ case, a structure in which Br ions are preferentially placed in equatorial positions was also tested (the "ordered structure"). These structures and their computed XAS are shown in Figure 4. The randomized structures for all compositions feature varying degrees of octahedral tilting (Figure S8), whereas the ordered structure for $x = 0.6$ displays significantly less. For $x = 0.6$, however, the spectrum of the randomized structure is a significantly better match to experiment. As seen in the P5 test above, the significant tilting of Pb cages disrupts the *d-d* couplings, broadening and slightly blueshifting the associated spectral features. This effect is strongest for the d_{z^2} state, which is oriented along the Pb-halide bonds and therefore highly sensitive to tilting motions.

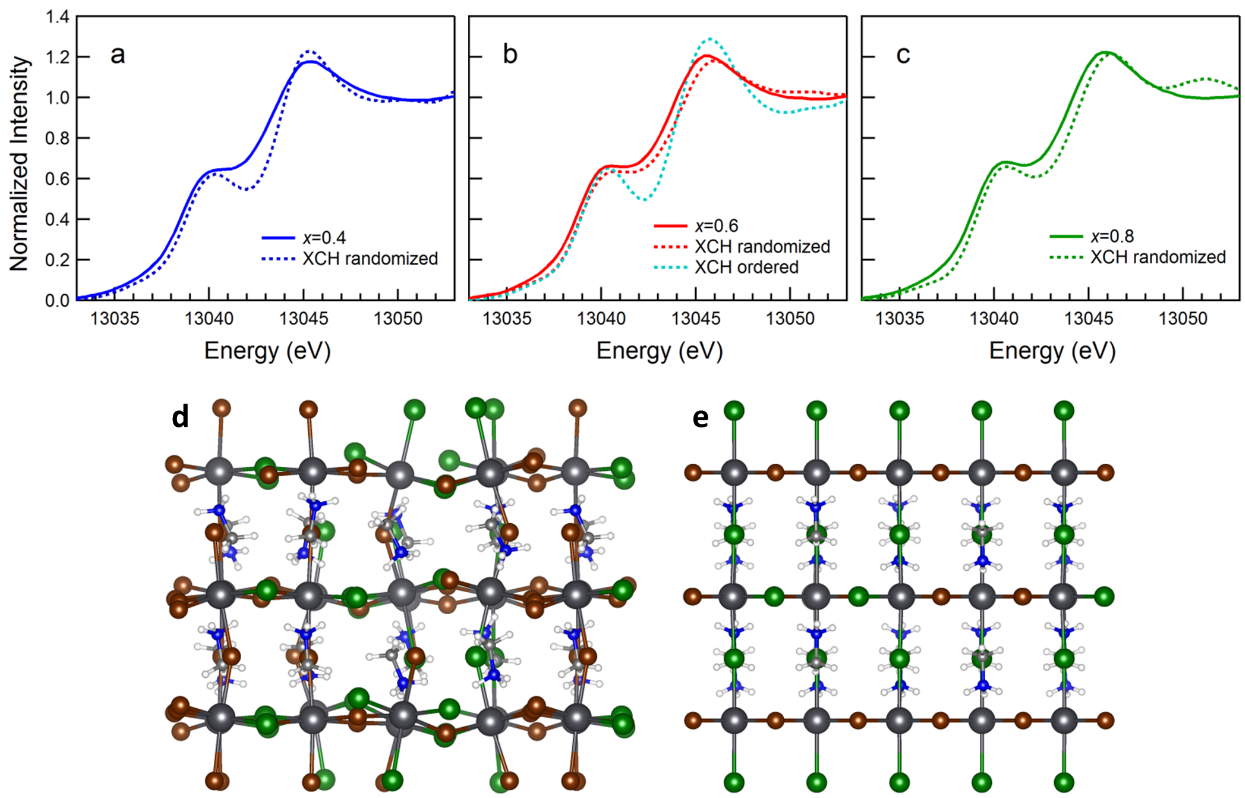

Figure 4: Experimental HERFD XAS compared to computed XAS for (a) the $x = 0.4$ perovskite, (b) the $x = 0.6$ perovskite, and (c) the $x = 0.8$ perovskite. For the $x = 0.6$ perovskite, computed spectra from two structures are shown: a structure with a randomized distribution of halides (dotted red line, structure shown in panel (d)) and an ordered structure in which Br ions preferentially occupy equatorial positions in the Pb octahedral (dotted cyan line, structure shown in panel (e)). Pb are dark grey, I are green, Br are brown, C are light grey, N are blue, and H are white.

These computed structures indicate that intermediate compositions between $MAPbI_3$ and $MAPbBr_3$ display greater degrees of octahedral tilting, but experimental spectra do not reflect this. The generally broadened spectral shapes observed for structures with larger degrees of octahedral tilting are seen experimentally across the entire composition range. Additionally, measured Urbach energies and photoluminescence quantum yield measurements do not imply any trends in structural distortion as a function of composition.[23-24] Given that the energy difference between the randomized and ordered structures for the $x = 0.6$ composition is only 0.08 eV per formula unit, we hypothesize that thermal motions dominate over any preferred static tilting for any halide composition. This small energy difference also indicates that there is little preference for ordered halides versus a random distribution, a conclusion supported by tests of a "clustered" structure for the $x = 0.6$ composition in which I and Br are grouped around different Pb atoms (Figure S9). The clustered structure displays similar octahedral tilts to the randomized structure, but produces a sharpened rising edge spectral feature that does not match experiment. This implies a random distribution of halides in the actual material.

The octahedral tilting motions discussed above also have a significant impact on the band gap. The randomized structure for the $x = 0.6$ composition has a computed DFT-PBE band gap 0.34 eV higher than the ordered structure. A systematic test of varying degrees of octahedral tilting between $MAPbBr_3$ and the tilted P5 structure is shown in Figure S10, revealing a dramatic increase in band gap of up to 0.57 eV for large amplitude tilts. Thermally induced tilting motions would therefore cause a net increase in band gap, by increasing the root mean square tilt angle around the equilibrium structure. This is conflated with thermal lattice expansion, which also affect the band gap (larger lattice parameters give larger band gaps), and the combination of the two effects may explain why observed band gaps in $MAPbI_3$ increase with temperature.[25-26] More accurate calculations of electronic and opto-electronic properties of these structural models may be provided by many-body perturbation theory,[27-28] but we expect the trends discussed here to be robust. Our HERFD XAS is sensitive to both lattice parameters (demonstrated with P3 vs. P4) and tilting motions, and can therefore provide a much-needed connection between these different structural degrees of freedom and their impacts on the observed effective band gap and basic optoelectronic properties, which impact charge carrier transport and stability in real devices.

Conclusion:

We have demonstrated that HERFD XAS at the Pb L_{III} absorption edge, coupled with first-principles DFT calculations, provides a highly local probe of electronic and atomic structure in mixed organo-lead halide perovskites. DFT structures allow testing of structural hypotheses to disentangle the effects of different degrees of freedom on the spectra, ultimately revealing the structural details embedded in the experimental HERFD XAS. This approach reveals that, for mixed I/Br perovskites, halides are randomly distributed throughout the structure and that thermal motions dominate over any preferred structural conformations as a function of composition. The spectra probe a ligand field splitting in the Pb and halide *d* states that lie above the conduction band minimum, but are highly sensitive to structural details including Pb-halide bond lengths, halide identity, and octahedral tilting. Combining HERFD XAS with DFT-based interpretation therefore provides a means to unravel these structural details, which underlie optoelectronic properties, including the effective bandgaps, of lead halide perovskites. This represents an important step in enabling nanoscale understanding – and eventually tailoring – structure-property relationships in the emerging class of hybrid organic-inorganic perovskites for high-efficiency solar energy conversion.

Acknowledgment:

This material is based upon work performed by the Joint Center for Artificial Photosynthesis, a DOE Energy Innovation Hub, supported through the Office of Science of the

U.S. Department of Energy under Award Number DE-SC0004993. Use of the Stanford Synchrotron Radiation Lightsource, SLAC National Accelerator Laboratory, is supported by the U.S. Department of Energy, Office of Science, Office of Basic Energy Sciences under Contract No. DE-AC02-76SF00515. DFT-based spectral simulations by Y.L. and D.P. were performed as a user project at the Molecular Foundry, and computing resources were provided by the National Energy Research Scientific Computing Center, both supported by the Office of Science, Office of Basic Energy Sciences, of the U.S. Department of Energy under Contract No. DE-AC02-05CH11231. L. L. and J. B. N. supported by the Director, Office of Science, Office of Basic Energy Sciences, Materials Sciences and Engineering Division, of the U.S. Department of Energy under Contract No. DE-AC02-05CH11231. L. L. also acknowledges partial financial support from the Feodor-Lynen program of the Alexander-von-Humboldt Foundation. C. M. S.-F. acknowledges financial support from the Swiss National Science Foundation (P2EZP2_155586).

References:

1. NREL Chart. *https://www.nrel.gov/pv/assets/images/efficiency-chart.png* **Accessed 2/15/2017**.
2. Poglitsch, A.; Weber, D. Dynamic disorder in methylammoniumtrihalogenoplumbates (II) observed by millimeter-wave spectroscopy. *The Journal of Chemical Physics* **1987,** *87* (11), 6373-6378.
3. Kawamura, Y.; Mashiyama, H.; Hasebe, K. Structural Study on Cubic-Tetragonal Transition of CH3NH3PbI3. *Journal of the Physical Society of Japan* **2002,** *71* (7), 1694-1697.
4. Noh, J. H.; Im, S. H.; Heo, J. H.; Mandal, T. N.; Seok, S. I. Chemical Management for Colorful, Efficient, and Stable Inorganic–Organic Hybrid Nanostructured Solar Cells. *Nano Letters* **2013,** *13* (4), 1764-1769.
5. Mosconi, E.; Amat, A.; Nazeeruddin, M. K.; Grätzel, M.; De Angelis, F. First-Principles Modeling of Mixed Halide Organometal Perovskites for Photovoltaic Applications. *The Journal of Physical Chemistry C* **2013,** *117* (27), 13902-13913.
6. Leppert, L.; Reyes-Lillo, S. E.; Neaton, J. B. Electric Field- and Strain-Induced Rashba Effect in Hybrid Halide Perovskites. *The Journal of Physical Chemistry Letters* **2016,** *7* (18), 3683-3689.
7. Leblebici, S. Y.; Leppert, L.; Li, Y.; Reyes-Lillo, S. E.; Wickenburg, S.; Wong, E.; Lee, J.; Melli, M.; Ziegler, D.; Angell, D. K.; Ogletree, D. F.; Ashby, Paul D.; Toma, F. M.; Neaton, J. B.; Sharp, I. D.; Weber-Bargioni, A. Facet-dependent photovoltaic efficiency variations in single grains of hybrid halide perovskite. *Nature Energy* **2016,** *1*, 16093.
8. Filip, M. R.; Eperon, G. E.; Snaith, H. J.; Giustino, F. Steric engineering of metal-halide perovskites with tunable optical band gaps. *Nature Communications* **2014,** *5*, 5757.
9. Grote, C.; Berger, R. F. Strain Tuning of Tin–Halide and Lead–Halide Perovskites: A First-Principles Atomic and Electronic Structure Study. *The Journal of Physical Chemistry C* **2015,** *119* (40), 22832-22837.
10. Hämäläinen, K.; Siddons, D. P.; Hastings, J. B.; Berman, L. E. Elimination of the inner-shell lifetime broadening in x-ray-absorption spectroscopy. *Physical Review Letters* **1991,** *67* (20), 2850-2853.
11. Prendergast, D.; Galli, G. X-ray absorption spectra of water from first principles calculations. *Physical Review Letters* **2006,** *96* (21), 215502.
12. Li, Y.; Cooper, J. K.; Buonsanti, R.; Giannini, C.; Liu, Y.; Toma, F. M.; Sharp, I. D. Fabrication of Planar Heterojunction Perovskite Solar Cells by Controlled Low-Pressure Vapor Annealing. *The Journal of Physical Chemistry Letters* **2015,** *6* (3), 493-499.
13. Wang, Y.; Lü, X.; Yang, W.; Wen, T.; Yang, L.; Ren, X.; Wang, L.; Lin, Z.; Zhao, Y. Pressure-Induced Phase Transformation, Reversible Amorphization, and Anomalous Visible Light Response in Organolead Bromide Perovskite. *Journal of the American Chemical Society* **2015,** *137* (34), 11144-11149.
14. England, A. H.; Duffin, A. M.; Schwartz, C. P.; Uejio, J. S.; Prendergast, D.; Saykally, R. J. On the hydration and hydrolysis of carbon dioxide. *Chemical Physics Letters* **2011,** *514* (4-6), 187-195.
15. Haynes, W. M. *CRC handbook of chemistry and physics*. CRC press: 2014.
16. Lee, J.-H.; Bristowe, N. C.; Bristowe, P. D.; Cheetham, A. K. Role of hydrogen-bonding and its interplay with octahedral tilting in CH3NH3PbI3. *Chemical Communications* **2015,** *51* (29), 6434-6437.
17. Lee, J. H.; Lee, J.-H.; Kong, E.-H.; Jang, H. M. The nature of hydrogen-bonding interaction in the prototypic hybrid halide perovskite, tetragonal CH(3)NH(3)PbI(3). *Scientific Reports* **2016,** *6*, 21687.
18. Bechtel, J. S.; Seshadri, R.; Van der Ven, A. Energy Landscape of Molecular Motion in Cubic Methylammonium Lead Iodide from First-Principles. *The Journal of Physical Chemistry C* **2016,** *120* (23), 12403-12410.
19. Kresse, G.; Furthmüller, J. Efficient iterative schemes for \textit{ab initio} total-energy calculations using a plane-wave basis set. *Physical Review B* **1996,** *54* (16), 11169-11186.

20. Leguy, A. M. A.; Frost, J. M.; McMahon, A. P.; Sakai, V. G.; Kockelmann, W.; Law, C.; Li, X.; Foglia, F.; Walsh, A.; O'Regan, B. C.; Nelson, J.; Cabral, J. T.; Barnes, P. R. F. The dynamics of methylammonium ions in hybrid organic–inorganic perovskite solar cells. *Nature Communications* **2015,** *6*, 7124.
21. Mattoni, A.; Filippetti, A.; Saba, M. I.; Delugas, P. Methylammonium Rotational Dynamics in Lead Halide Perovskite by Classical Molecular Dynamics: The Role of Temperature. *The Journal of Physical Chemistry C* **2015,** *119* (30), 17421-17428.
22. Bellaiche, L.; Vanderbilt, D. Virtual crystal approximation revisited: Application to dielectric and piezoelectric properties of perovskites. *Physical Review B* **2000,** *61* (12), 7877-7882.
23. Sutter-Fella, C. M.; Miller, D. W.; Ngo, Q. P.; Roe, E. T.; Toma, F. M.; Sharp, I. D.; Lonergan, M. C.; Javey, A. Band Tailing and Deep Defect States in CH3NH3Pb(I1-xBrx)3 Perovskites as Revealed by Sub-Bandgap Photocurrent. *ACS Energy Letters* **2017**.
24. Sutter-Fella, C. M.; Li, Y.; Amani, M.; Ager, J. W.; Toma, F. M.; Yablonovitch, E.; Sharp, I. D.; Javey, A. High Photoluminescence Quantum Yield in Band Gap Tunable Bromide Containing Mixed Halide Perovskites. *Nano Letters* **2016,** *16* (1), 800-806.
25. Foley, B. J.; Marlowe, D. L.; Sun, K.; Saidi, W. A.; Scudiero, L.; Gupta, M. C.; Choi, J. J. Temperature dependent energy levels of methylammonium lead iodide perovskite. *Applied Physics Letters* **2015,** *106* (24), 243904.
26. Milot, R. L.; Eperon, G. E.; Snaith, H. J.; Johnston, M. B.; Herz, L. M. Temperature-Dependent Charge-Carrier Dynamics in CH3NH3PbI3 Perovskite Thin Films. *Advanced Functional Materials* **2015,** *25* (39), 6218-6227.
27. Reyes-Lillo, S. E.; Rangel, T.; Bruneval, F.; Neaton, J. B. Effects of quantum confinement on excited state properties of ${\mathrm{SrTiO}}_{3}$ from ab initio many-body perturbation theory. *Physical Review B* **2016,** *94* (4), 041107.
28. Filip, M. R.; Hillman, S.; Haghighirad, A. A.; Snaith, H. J.; Giustino, F. Band Gaps of the Lead-Free Halide Double Perovskites Cs2BiAgCl6 and Cs2BiAgBr6 from Theory and Experiment. *The Journal of Physical Chemistry Letters* **2016,** *7* (13), 2579-2585.